Thermal enhancement of the antiferromagnetic exchange coupling between Fe epilayers separated by a crystalline ZnSe spacer

2006 J. Phys.: Condens. Matter 18 9105

(http://iopscience.iop.org/0953-8984/18/39/036)

INSTITUTE OF PHYSICS PUBLISHING JOURNAL OF PHYSICS: CONDENSED MATTER

J. Phys.: Condens. Matter **18** (2006) 9105–9118 doi:10.1088/0953-8984/18/39/036

Thermal enhancement of the antiferromagnetic exchange coupling between Fe epilayers separated by a crystalline ZnSe spacer

J Varalda[1], J Milano[2], A J A de Oliveira[1], E M Kakuno[3], I Mazzaro[3], D H Mosca[3], L B Steren[2], M Eddrief[4], M Marangolo[4], D Demaille[4] and V H Etgens[4]

[1] Departamento de Física, Universidade Federal de São Carlos, CP 676, 13565-905 São Carlos SP, Brazil
[2] Centro Atómico Bariloche, Comisión Nacional de Energía Atómica and Instituto Balseiro, Universidad Nacional de Cuyo, Av. E. Bustillo 9500, (8400) S. C. de Bariloche, Argentina
[3] Departamento de Física, Universidade Federal do Paraná, C. Pl. 19091, 81531-990 Curitiba PR, Brazil
[4] INSP, Université Pierre et Marie Curie-Paris6, Université Denis Diderot-Paris7, CNRS, UMR 7588 Campus Boucicaut, 140 rue de Lourmel, 75015 Paris, France

E-mail: milano@cab.cnea.gov.ar

Received 20 April 2006, in final form 19 July 2006
Published 15 September 2006
Online at stacks.iop.org/JPhysCM/18/9105

Abstract

We provide evidence for the existence of an antiferromagnetic coupling between iron epilayers separated by a wedge-like ZnSe crystalline semiconductor by magnetometric and ferromagnetic resonance experiments. The coupling strength of 46 μJ m^{-2} for $t_{ZnSe} = 25$ Å is strongly reduced as the barrier thickness is increased. The coupling increases linearly with temperature from 5 to 300 K, with a 5.5×10^{-9} J m^{-2} K^{-1} rate. Thermally induced effective exchange coupling mediated by spin-dependent tunnelling of electrons via localized mid-gap defect states in the ZnSe spacer layer appears to be the most plausible mechanism to induce the antiferromagnetic coupling.

1. Introduction

The special interest in hybrid ferromagnet/semiconductor heterostructures arises from their plausible wide uses in spintronic devices. The active research on compatible materials to integrate complex structures and the finding of optimal growth conditions have caused these new materials to reach technological standards for their application.

Generally speaking, these junctions are complex magnetic systems in which interface magnetic anisotropies, shape induced anisotropies, and interlayer magnetic coupling can play a major role in the magnetic response of the system. The study of these phenomena needs well characterized systems presenting sharp interfaces, not always found in metal/semiconductor

junctions. In this paper we present experimental work on a particularly unreactive interface tunnel junction, i.e. Fe/ZnSe/Fe.

The magnetic coupling between two ferromagnetic layers across a non-ferromagnetic spacer has been intensively investigated in the last years, both experimentally and theoretically. Early results have shown an oscillatory ferromagnetic/antiferromagnetic coupling in metallic multilayers [1] as a function of the spacer thickness. This kind of coupling cannot be simply explained by the Rudderman–Kittel–Kasuya–Yoshida (RKKY) model as was initially proposed, but its physical origin has been attributed to quantum interferences due to spin-dependent reflections at the spacer boundaries [2–4]. The quantum well state (QWS) nature of the interlayer coupling in metallic systems was experimentally confirmed by magnetic measurements [5, 6] and photoemission experiments [7–9]. The observation of an oscillatory behaviour of the interlayer exchange coupling (IEC) as a function of the ferromagnetic layer thickness [5, 6] and a strong temperature dependence of (IEC) strength support QWS models [10]. Bruno [2] showed that the quantum interference effects can be included in a modified RKKY model. He also proposed a unified treatment of the interlayer coupling through metallic and insulating spacer layers, by introducing the concept of a complex Fermi surface.

Whereas Bruno's theory applies to crystalline systems, in most cases the experimental finding addresses the exchange coupling across non-metallic spacers in polycrystalline and even amorphous materials, namely a-Si [11], a-Ge [12], and a-ZnSe [13]. High-quality epitaxial semiconductor EuS/PbS/EuS trilayers exhibit antiferromagnetic coupling, but their strength decreases with temperature consistently with a power-law dependence of the EuS magnetization [14]. Other semiconductor epitaxial systems, such as (Ga, Mn)As/(Al, Ga)As/(Ga, Mn)As [15] and (Ga, Mn)As/InAs/(Ga, Mn)As [16], are ferromagnetically exchange coupled for a rather long spacer thickness range, typically around 300 Å. Moreover, strong antiferromagnetic coupling, exponentially decaying with the thickness of the spacer, has been observed for Fe/Si/Fe epitaxial structures [17]. However, the high chemical reactivity at the Fe/Si interfaces always complicates the physics of the system. Concrete experimental evidence of room-temperature antiferromagnetic interlayer coupling by equilibrium quantum tunnelling of spin-polarized electrons between the ferromagnetic layers has been reported on epitaxial MgO(100)/Fe/MgO/Fe/Co magnetic tunnel junctions [18].

In this paper, we present a detailed study of the interlayer magnetic coupling across a semiconductor barrier as a function of the spacer thickness and temperature. With this purpose, we have grown trilayers with bottom and top iron layers separated by a ZnSe epilayer with a continuously variable thickness (wedge). Such a wedge allows us to rule out growth unavoidable deviations from one sample to another that are present in the case of series of samples prepared with different thickness. We would like to emphasize that the Fe/ZnSe system is a rare successful example of ferromagnetic metal–semiconductor epitaxy in which the chemistry and magnetic properties of the abrupt Fe/ZnSe(001) interfaces remain stable up to 300 °C [19].

2. Experimental details

The Fe/ZnSe/Fe samples were prepared by molecular beam epitaxy (MBE) in a multi-chamber growth system. First, a 3000 Å thick undoped GaAs buffer layer was grown onto a GaAs(001) substrate with stabilization of the $\beta(2 \times 4)$ As-rich reconstruction at the end of the growth. The samples were then quickly transferred under ultra-high-vacuum conditions to the II–VI growth chamber where an undoped 100 Å ZnSe epilayer was also deposited at 220 °C using

alternate layer epitaxy [20]. The $c(2 \times 2)$ Zn-rich surface was stabilized at the end of the growth. Over this reconstructed surface the bottom iron layer was grown (65 Å thick) at 180 °C using a Knudsen cell with a grown rate of about 1.4 Å min^{-1}. Next, the ZnSe wedge was deposited at 220 °C following the specific procedure already described elsewhere [21]. The wedge thickness varies between 25 and 80 Å, with a slope of about 1–2 Å mm^{-1} and oriented along the ZnSe [110] direction. Finally, the top iron layer was deposited with a thickness of 140 Å and substrate temperature of 180 °C. A gold cap layer deposited at room temperature was used to protect the samples against air exposure. The wedge was cleaved into thin slices, perpendicular to the wedge direction.

We have also studied trilayers [22, 23] with constant and homogeneous ZnSe thickness, between 30 and 80 Å, in order to check the reproducibility of our results obtained in the wedge sample. Thin reference Fe layers were also grown in order to determine the magnetic parameters for isolated single layers. Reflection high-energy electron diffraction (RHEED), x-ray photoelectron spectroscopy (XPS) [24], x-ray magnetic circular dichroism (XRD) [19] and *in situ* scanning tunnelling microscopy (STM) facilities have been used to characterize the growth of the samples.

The magnetic measurements were carried out in a SQUID magnetometer. The field was applied parallel to the film plane along the crystallographic axis of the substrate. From a phenomenological point of view, magnetic coupling between magnetic layers separated by a non-magnetic one may be expressed in powers of internal product of the magnetization unit vectors (i.e. cosine of angle) of each interacting layer. When the angle between the magnetization of one layer with respect to the other one is θ, the IEC per unit area may be written as $J = J_1 \cos\theta + J_2 \cos^2\theta + \cdots$, where J_1 is the effective Heisenberg coupling constant, and J_2 is the so-called biquadratic coupling. The magnetic coupling strength can be quantitatively estimated from the external magnetic field necessary to compensate the effective exchange field between the ferromagnetic layers. We have used the *minor hysteresis loops* method to evaluate the magnetic coupling between the Fe layers. In this method, once the magnetization direction of the hard ferromagnetic layer is fixed, minor loops are measured sensing only the magnetization of the softer ferromagnetic layer. If there is a magnetic coupling between the ferromagnetic layers, the minor loop is displaced along the field axis. The net sign of the displacement with respect to the zero-coupling position, positive or negative, results in an evidence of a ferromagnetic (F) or antiferromagnetic (AF) coupling, respectively. The shift modulus is known as the compensation field (H_{comp}) and corresponds to the magnetic field at which the magnetostatic energy of the softer magnetic layer and the coupling energy between layers are identical. We have assumed that the coupling is bilinear (Heisenberg), so the constant J was quantitatively estimated as the energy difference, per unit area, between the parallel and antiparallel magnetization alignment; i.e., $J = \frac{1}{2} t_F \cdot M_S \cdot H_{comp}$ with t_F being the magnetic softer layer thickness.

In our measurements, the magnetic field is determined by converting the current applied to the superconducting coil. As the compensation and coercive fields involved in the problem are comparable with the typical remanent fields (H_{rem}) of the superconducting coil, a systematic procedure was employed to minimize and to estimate H_{rem}. This field was measured using a Hall probe at the sample position. The remanent field measured for the ± 1.5 kOe field loop used in our experiments is (1.50 ± 0.25) Oe. This H_{rem} value was used to correct the current-converted measured magnetic field in the low field region.

Ferromagnetic resonance experiments were performed at Q-band ($\sim$33 GHz) in a Bruker spectrometer. The angular dependence of the resonance spectra was studied in the in-plane ([100] to [010]) geometry at room temperature.

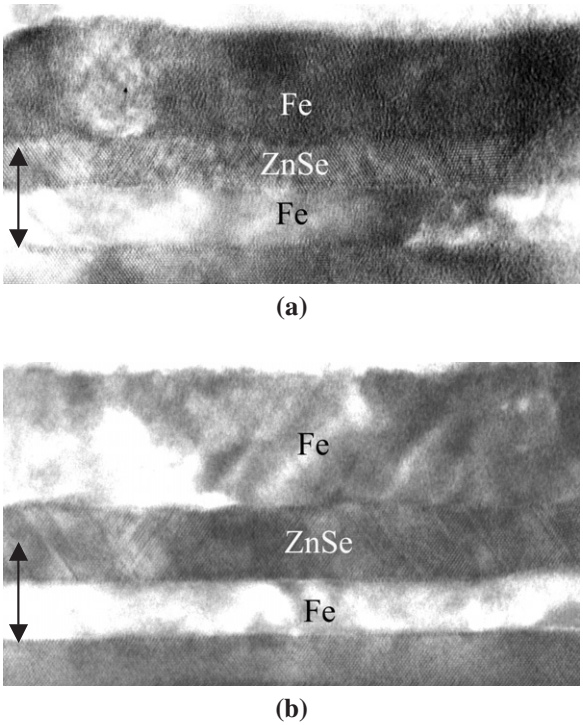

Figure 1. Cross-sectional TEM image of Fe 140 Å/ZnSe t_{ZnSe}/Fe 65 Å structures for t_{ZnSe} 40 Å (a) and 80 Å (b). The arrows indicate the 100 Å vertical scale.

3. Results

We will first describe the structure and interface morphology of the Fe/ZnSe-wedge/Fe epilayers. Next, the magnetic properties of the Fe/ZnSe/Fe trilayer will be presented. The existence of a magnetic coupling strength across the ZnSe spacer, as well as its dependence with the barrier thickness and temperature, will be shown.

3.1. Structural characterization

The first Fe layer grows epitaxially on top of the pseudomorph ZnSe(001) thin epilayer grown on GaAs(001) substrate. According to RHEED and XPS analysis, the 65 Å thick Fe(001) films are completely relaxed and display high quality and uniformity [24]. The STM images display a surface morphology of Fe epilayers with very small roughness at micrometric scale. The crystalline ZnSe(001) epilayer with a wedge shape on top of this first Fe layer was monitored by *in situ* RHEED experiments. The thickness profile of the wedge was also controlled by transmission electron microscopy (TEM). Figure 1 shows cross-sectional TEM images of samples with $t_{ZnSe} = 40$ Å and $t_{ZnSe} = 80$ Å; abrupt and atomically flat Fe/ZnSe and reverse ZnSe/Fe interfaces can be clearly observed. In both cases, the ZnSe spacer layer is rather uniform and shows no evidence of pinholes or disruptive defects. The top Fe layers exhibit a poorer crystalline quality in comparison to the bottom one regarding structural disorder, and defects homogeneously distributed along the iron epilayer can be observed. In spite of these characteristics, our group have reported in [25] the epitaxial growth of Fe films above 27 ML prepared by MBE and in similar conditions to our trilayers (in our samples the Fe layers are 45 and 97 ML thick).

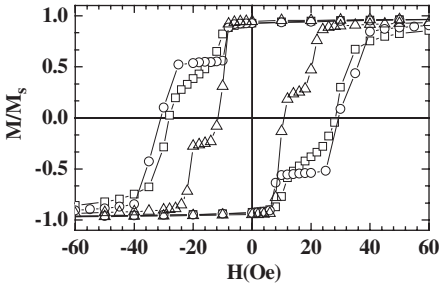

Figure 2. Magnetization loops for samples Fe/ZnSe t_{ZnSe}/Fe with $t_{ZnSe} = 25$ Å (square), 37 Å (circle), and 45 Å (triangle), measured at room temperature. The magnetic field was applied parallel to the [100] direction.

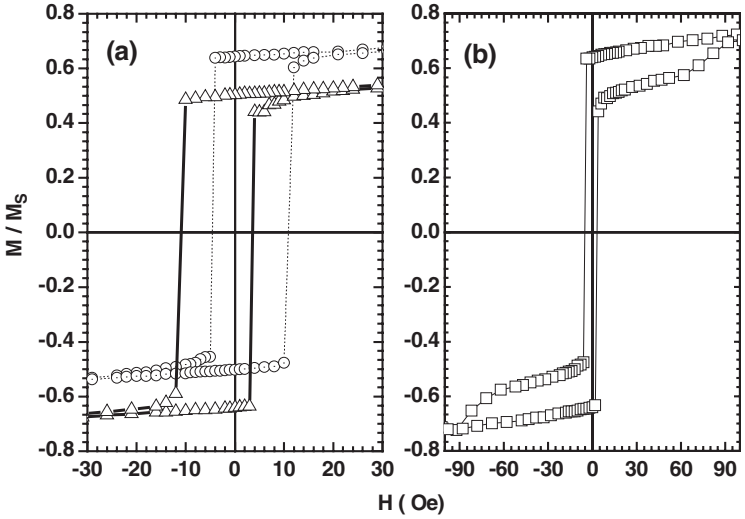

Figure 3. (a) Minor loops for Fe/ZnSe 40 Å/Fe measured with positive saturation field (circle) and negative saturation field (triangle). (b) Low-field region of the major magnetization loop of the same sample. The measurements were carried out at room temperature.

3.2. Magnetization measurements

In figure 2 the magnetization versus applied field curves for Fe/ZnSe t_{ZnSe}/Fe samples with $t_{ZnSe} = 25, 37$ and 45 Å are shown. The two-step magnetization loop observed in all the samples is associated with the magnetization reversal of the top and bottom layers. This feature suggests that the iron layers are either uncoupled or weakly coupled. To clarify this aspect minor loops have been performed. Figure 3(a) shows a typical result performed in our samples with $t_{ZnSe} \geqslant 40$ Å. A slight shift of the minor loops to negative H_{comp}, i.e., a weak antiferromagnetic coupling between Fe layers, is observed in the figure. The low field magnetization loop of the sample is shown in figure 3(b). Similarly a small antiferromagnetic coupling is observed by SQUID measurements for all the samples with ZnSe thickness varying from 40 to 80 Å. For $t_{ZnSe} < 40$ Å the H_{comp} becomes quite similar to the switching field of the hardest Fe layer and the *minor hysteresis loops* method cannot be unambiguously used. Thereafter, the magnetic coupling between the Fe layers, J, was quantitatively estimated from H_{comp} for samples with $t_{ZnSe} > 40$ Å and these results are plotted in figure 4.

Figure 5 shows the temperature dependence of the magnetic coupling for $t_{ZnSe} = 40$ and 80 Å, deduced from SQUID measurements. As can be seen, the coupling strength increases linearly with temperature and the slope is approximately the same for the two samples. A variation of the interlayer coupling with temperature has been predicted by Bruno in his model [2]. The temperature dependence of the IEC across metallic and non-metallic spacer layers is currently ascribed to two mechanisms: (i) thermal excitations of electron–hole pairs

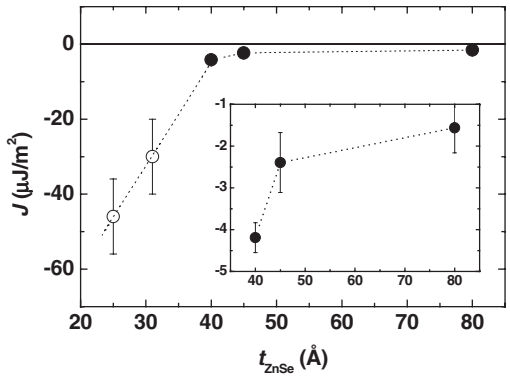

Figure 4. Room-temperature magnetic coupling strength as a function of the ZnSe spacer layer, deduced from magnetization (filled circle) and ferromagnetic resonance (open circle) measurements. Negative J values indicate antiferromagnetic coupling. The inset shows SQUID measurements in an enlarged scale.

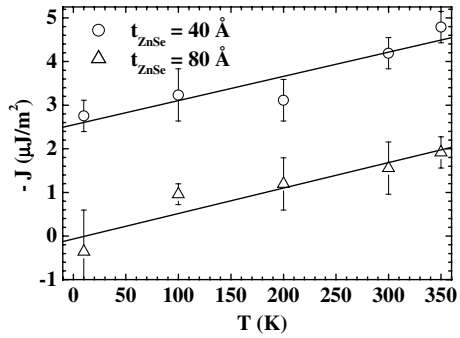

Figure 5. Temperature dependence of the antiferromagnetic coupling for the trilayers with $t_{\mathrm{ZnSe}} = 40$ and 80 Å. The slope of both curves is $\sim 5.5 \times 10^{-9}$ J m^{-2} K^{-1}.

across Fermi level as described by the Fermi–Dirac function, and (ii) thermal excitation of spin waves in the magnetic layers and particularly at their interfaces. Specifically, for a ZnSe semiconducting spacer layer the former mechanism is extended to include (a) spin-dependent thermal repopulation of levels close to the Fermi surface through the hybridization of metallic states with localized weakly bound electron states situated at or near to the two interfaces [26], and (b) spin-dependent thermal population of impurity/defect mid-gap states via resonant and non-resonant tunnelling [27]. A further discussion of this effect is given in section 4.

3.3. Ferromagnetic resonance measurements

The ferromagnetic resonance (FMR) spectra were measured with the static magnetic field applied in the plane of the samples. The spectra are composed of two resonance modes, as shown in figure 6 for two samples of different ZnSe spacer thickness. In the following we will discuss samples with $t_{\mathrm{ZnSe}} = 45$ and 25 Å (figures 6(a) and (b)) whose spectra are representative for all the measured samples with $t_{\mathrm{ZnSe}} \geqslant 40$ Å and $t_{\mathrm{ZnSe}} \leqslant 31$ Å, respectively. We notice in both cases that the resonance fields depend on the in-plane direction of the magnetic field and also the intensity and the overall shape of the lines. The FMR spectra of samples with larger ZnSe thickness are shifted to lower fields when the magnetic field is rotated from the [110] to the [100] direction (figure 6(a)). In contrast, in the spectra of samples with $t_{\mathrm{ZnSe}} \leqslant 31$ Å, only one resonance mode changes its resonance field and its intensity increases when the magnetic field angle is rotated from the [110] to the [100] direction (figure 6(b)). The resonance mode whose intensity is larger is associated to the thicker layer (top) and the other one to the thinner layer (bottom), based on the proportionality between the resonance line intensity and magnetization [28].

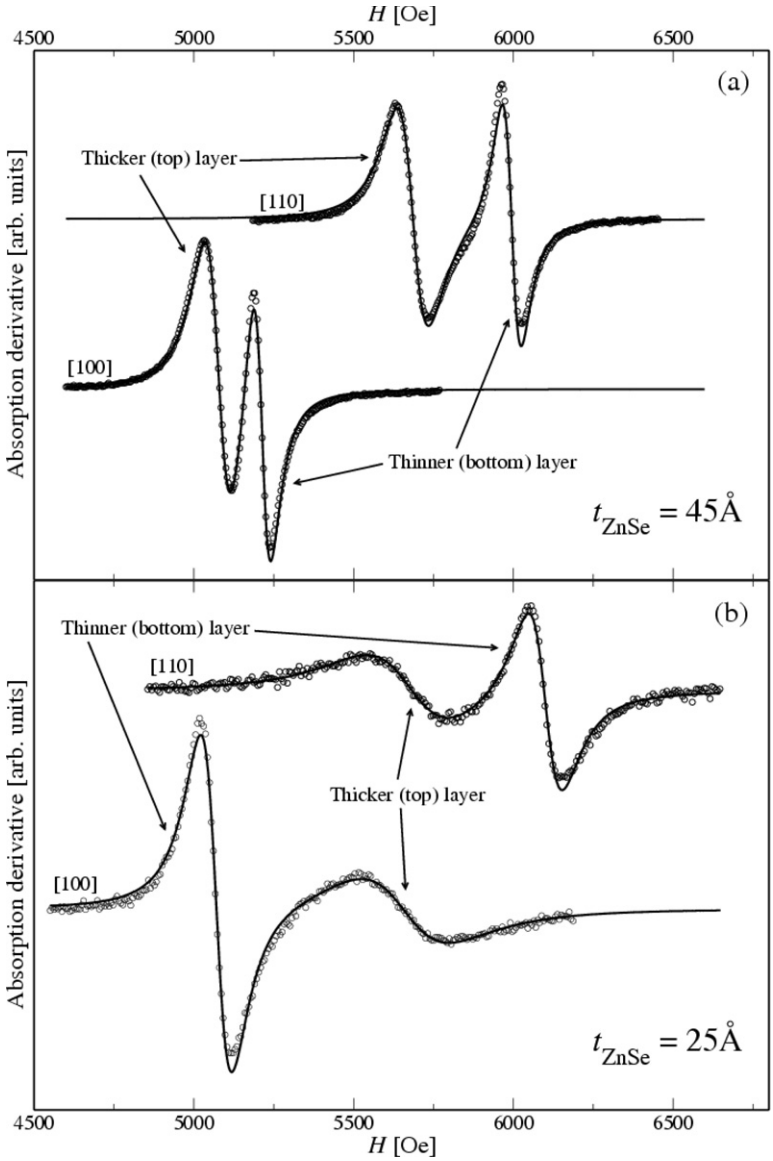

Figure 6. FMR spectra of the trilayers with spacer thickness (a) $t_{ZnSe} = 45$ Å and (b) $t_{ZnSe} = 25$ Å. The static magnetic field was applied along the [110] and [100] directions.

The in-plane (IP) angular dependence of the resonance fields for the Fe/ZnSe/Fe samples with $t_{ZnSe} = 45$ Å and $t_{ZnSe} = 25$ Å is presented in figures 7(a) and (b), respectively. In figure 7(a) we observe two curves, associated to the mode of each iron layer. From these plots we see that the resonance fields have a four-fold symmetry, attributed to the magnetocrystalline anisotropy of the iron bcc structure. This behaviour changes for the samples with thinner ZnSe barriers: the resonance field of the top layer remains almost constant at 5.8 kOe as a function of φ_H, whereas the mode of the bottom layer presents the same behaviour observed in the former samples. The data of the bottom layer are absent in some angular intervals because, in those ranges, the two resonance lines merge into a single one. In both samples,

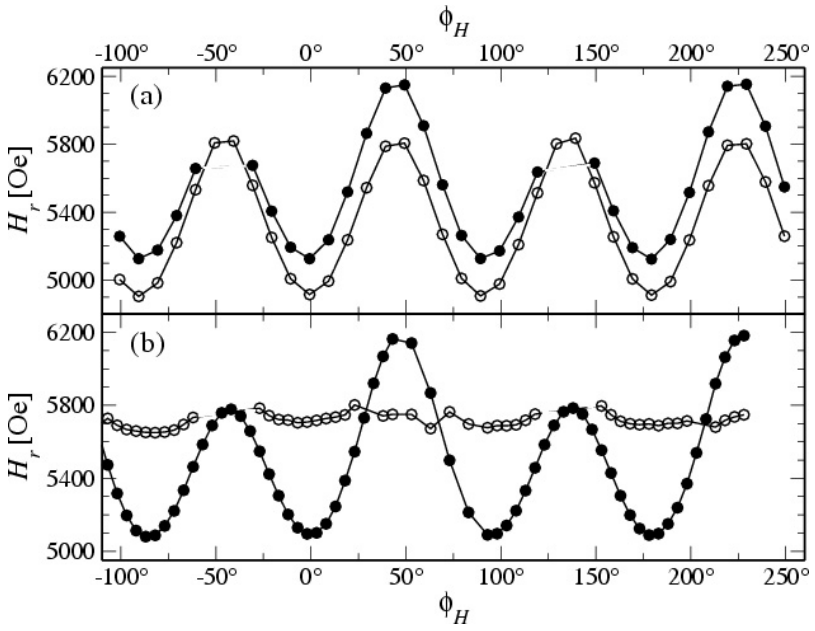

Figure 7. Resonance fields as a function of the azimuthal angle of the external field, φ_H, for samples with (a) $t_{\mathrm{ZnSe}} = 45$ Å and (b) $t_{\mathrm{ZnSe}} = 25$ Å. The resonance fields associated with the top and bottom iron layers are plotted with open and filled symbols, respectively.

a small in-plane uniaxial anisotropy is measured for the bottom layer. This contribution is induced at the ZnSe/Fe interface and has been previously reported for ZnSe/Fe and GaAs/Fe structures [23, 25, 29]. This kind of anisotropy is not observed in the thicker iron layer, probably due to its interfacial origin.

In general, the coupling [28] between magnetic layers changes the position of the resonance field, H_{r}, and the linewidth, ΔH, of the FMR modes. However, in our case, due to the small coupling present, there is no measurable change in these parameters. For instance, the order of magnitude of the shift of the resonance mode induced by a magnetic coupling smaller than 100 μJ m^{-2} is tens of oersteds (this can be evaluated using equation (4)); thereafter the linewidths ($\Delta H \sim 140$ Oe and $\Delta H \sim 200$ Oe for the bottom and top layers, respectively) and the measurement noise hide these small resonance field variations. Moreover, we do not observe any systematic change associated with coupling in the linewidth as a function of the spacer thickness.

So, taking into account that in our samples the shift of the resonance field due to the interlayer coupling cannot be determined, we propose the following expression for the free energy density for the iron layers denoted by $i = t$ (top) and b (bottom) respectively, without including any coupling term:

$$F_i = -\mu_0 \mathbf{H}\cdot\mathbf{M}_i + \tfrac{1}{4}K_{4,i}\left[\sin^2(2\theta) + \sin^4(2\varphi)\right] + \tfrac{1}{2}M_{\mathrm{eff},i}^2\cos^2\theta + K_{\mathrm{u},i}\cos^2(\varphi - \varphi_{\mathrm{u},i})\sin^2\theta, \quad (2)$$

where θ is the polar angle between $\mathbf{M}_i$ and the normal to the film plane, and φ is the azimuthal angle between $\mathbf{M}_i$ and the [100] direction. The first term is the Zeeman interaction of the iron moments $\mathbf{M}_i$ with the external magnetic field $\mathbf{H}$ and the second term describes the four-fold anisotropy coming from the iron bcc structure. The third term in the free energy density corresponds to the shape anisotropy corrected by a uniaxial anisotropy contribution,

K_n, that favours an out-of-plane (OOP) orientation of the magnetization. $M_{\rm eff}$ is an effective magnetization, given by $M_{\rm eff}^2 = M^2 - 2K_n$. As a consequence, the higher the K_n value is, the stronger is the shift towards higher resonance fields. Since K_n arises mainly from interfacial magnetostriction [25], its effect becomes more important for thinner magnetic layers. From this fact we corroborate our previous conclusion that the mode corresponding to thinner Fe layer is the one with higher resonance field in figure 6(a). The different behaviour observed in samples with thinner spacers will be discussed below. The last term corresponds to an in-plane uniaxial anisotropy $K_{\rm u}$, and $\varphi_{\rm u}$ is the angle between the uniaxial in-plane direction and the [100]. The equilibrium angles of M are obtained from the minimization of F.

The resonance frequency is given by [30]

$$\left(\frac{\omega}{\gamma}\right)^2 = \frac{1}{M^2 \sin^2\theta}\left[F_{\theta\theta}F_{\varphi\varphi} - F_{\theta\varphi}^2\right] \tag{3}$$

where the subscripts indicate partial derivatives, evaluated at the equilibrium angles θ_0 and φ_0; $\gamma = g \cdot \mu_{\rm B}/\hbar$ is the gyromagnetic ratio and $\omega = 2\pi\nu$.

The changes of the anisotropy constants of the bottom Fe layer along the samples are very small, being $K_{4,\rm b} = (4.5 \pm 0.3) \times 10^4$ J m^{-3} and $K_{\rm u,b} = (1.5 \pm 0.1) \times 10^4$ J m^{-3}, very similar to those obtained for single iron films [23]. Surprisingly, as the spacer layer thickness decreases, a strong depression of the calculated Fe top layer anisotropy, $K_{4,\rm t}$, is observed in our samples. This anisotropy constant changes from $(4.5 \pm 0.3) \times 10^4$ J m^{-3} for $t_{\rm ZnSe} \geqslant 40$ Å to $(0.5 \pm 0.1) \times 10^4$ J m^{-3} for $t_{\rm ZnSe} \leqslant 31$ Å. We attribute this effect to the existence of a strong induced interfacial anisotropy that hides the four-fold Fe magnetocrystalline bulk anisotropy. Probably, a few ZnSe monolayers between Fe layers are not enough to relax the stress originated at the Fe$_{\rm b}$/ZnSe interface. This fact is also reflected in the poorer crystalline quality of the top Fe layer with respect to the bottom one, as observed by TEM (figure 1).

The $K_{n,\rm b}$ and $K_{n,\rm t}$ constants change by around 20% among the different samples, -2.8×10^5 J m^{-3} being the average value for both Fe layers. The dispersion of the K_n values along the samples is high enough to hide any systematic change in the resonance field due to coupling. In fact, the dependence of the resonance field on both parameters (coupling and K_n) is very similar. This reinforces our assumption of neglecting the coupling term from equation (2).

In spite of the fact that we do not notice coupling effects on the resonance fields and linewidth of the resonance spectra, important changes of the intensity ratio, $I_{\rm b}/I_{\rm t}$, with the spacer thickness of the samples are observed. This effect is clearly seen in figure 6(b), in which the $I_{\rm b}/I_{\rm t}$ ratio becomes smaller when the magnetic field is rotated from the [100] to [110] direction. The mode intensity is very sensitive to external factors, i.e. the microwave amplitude, and the sample's size, as well as to internal parameters of the spectrometer. However, very careful measurements can give a good estimation of the interlayer coupling.

In order to model the line intensity for the coupled case, we solved the Landau–Lifshitz equation of motion [28],

$$\frac{{\rm d}\mathbf{M}_{\rm t(b)}}{{\rm d}t} = \gamma\mathbf{M}_{\rm t(b)} \times \left(\mathbf{H}_{\rm eff,t(b)} + \frac{\lambda_{\rm t(b)}}{M^2}\mathbf{M}_{\rm t(b)} \times \mathbf{H}_{\rm eff,t(b)} + \frac{J}{t_{\rm t(b)}M^2}\mathbf{M}_{\rm b(t)}\right), \tag{4}$$

with a damping term which takes into account the relaxation of the magnetization and a last term of bilinear exchange coupling between the iron layers.

$\lambda_{\rm t(b)}$ is the damping parameter and its value is obtained by fitting the experimental linewidth for each Fe layer. The effective field $\mathbf{H}_{\rm eff}$ stands for all the contributions to the magnetic field present in the sample and is given by

$$\mathbf{H}_{\rm eff} = \mathbf{H} + \mathbf{h}_0 + \mathbf{H}_{\rm d} + \mathbf{H}_{\rm a}$$

where $\mathbf{H} = H\hat{x}$ is the dc magnetic field and $\mathbf{h}_0 = h_0 e^{i\omega t}\hat{y}$ is the rf one, $\mathbf{H}_d$ is the demagnetizing field and $\mathbf{H}_a$ takes into account the anisotropies of the system.

By linearizing this equation, including the field dependences explicitly, we have derived the susceptibility χ, of the time-dependent (rf) component of $\mathbf{M}$, $\mathbf{M}_{rf,i}$ given by χ, which is dM/dh_0 is related to the measured spectra through the absorbed power according to the following expression:

$$P(H) = \tfrac{1}{2}\omega \ \mathrm{Im}(\chi)|h_0|^2. \tag{5}$$

The field dependence of the absorbed power is proportional to the resonance line shape, as we show in figure 6. The measured spectra were fitted by equation (5), and in this way their intensity was related to the coupling constant J. A rigorous study must include the spin boundary conditions to solve equation (4). In particular, the border conditions are crucial for the treatment of exchange effects due to non-uniform magnetization within each magnetic layer [31, 32]. The non-uniform magnetization is mainly caused by the rf field skin depth and also the external torques induced, for example, by couplings. However, as is stated in [33], the exchange forces have no effect on the FMR spectra in a uniformly magnetized sample and this happens when the magnetic layer thicknesses are smaller than the microwave penetration depth. This is our case: the magnetic layer thicknesses are around 100 Å while a typical skin depth for a ferromagnetic material is ∼1000 Å. So, we assume that the variation of the magnetization within the layers is negligible and it has no effect over the FMR parameters.

In the case of uncoupled systems, the intensity of each line is proportional to the magnetic moment of the individual layer. On the other hand, when the system is coupled, the intensity of the modes depends on the strength of the coupling because each mode is composed of the ion's precession in both layers. In a coupled trilayer, the spectra are composed of two normal modes, commonly named acoustic and optical [28]. The acoustic mode corresponds to the in-phase precession of the magnetic moment of both layers and it leads to a parallel alignment of $\mathbf{M}_{rf,b}$ and $\mathbf{M}_{rf,t}$. On the other hand, the optical mode corresponds to the out-of-phase precession and the $\mathbf{M}_{rf,i}$ components are arranged in an antiparallel configuration. The intensity of each mode depends now on the net magnetic moment of the sample, $\mathbf{M}_{rf,b} - \mathbf{M}_{rf,t}$. Due to the parallel alignment of the $\mathbf{M}_{rf,i}$, the acoustic mode intensity is larger than that of the optical one in which the net magnetic moment is reduced due to the antiparallel configuration. It is important to note that these statements are independent of the coupling sign, i.e. ferromagnetic (FM) or antiferromagnetic (AF).

Our FMR results were analysed within this frame. The angular dependence of the intensity ratio, I_b/I_t, indicates that the net magnetic moment for each mode and therefore, the $\mathbf{M}_{rf,i}$ of one of the layer with respect to the other one, changes with the field direction. In figure 6(b), the smaller value of I_b for the [100] direction shows that the $\mathbf{M}_{rf,i}$ are aligned antiparallel (optical mode), whereas for the [110] direction they are aligned parallel (acoustic mode). The mode associated to the top layer presents the opposite behaviour. It is important to note that the change of the character mode (from acoustic to optical and vice versa) notably enhances the sensibility of the line intensities to the coupling. This effect is not remarkable in the other parameters, i.e. linewidth and resonance field. On the other hand, for samples with $t_{ZnSe} \geqslant 40$ Å, the modes do not change their relative position; then each mode, b and t, keeps its character (acoustic or optical) for every field direction. Therefore, in these samples, there is no enhancement of the intensity sensibility and the coupling measurement becomes difficult as it is via resonance field shift or linewidth changes.

At this point we have shown that the system is coupled because the ions of the two layers are participating in both modes, but we have said nothing about the sign of coupling. In figure 8, the ratio I_b/I_t is plotted as a function of the coupling constant strength for $\mathbf{H}$ applied in the

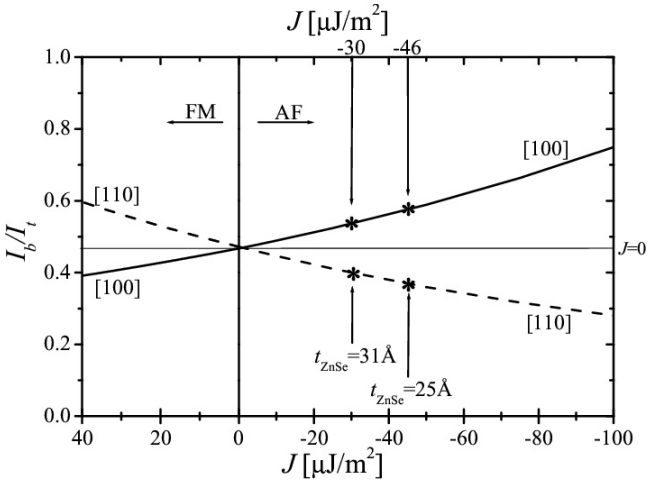

Figure 8. Calculated I_b/I_t as a function of the coupling strength for both ferromagnetic and antiferromagnetic coupling. The arrows show the measured ratios for Fe/ZnSe t_{ZnSe}/Fe trilayers with $t_{ZnSe} = 25$ and 31 Å samples. The horizontal line indicates the intensity ratio expected for an uncoupled system.

[100] and [110] directions. I_b/I_t has been calculated from equation (5) using the anisotropy constants obtained from the free layer spectra simulations. We can see that the curve depends on the coupling. For AF coupling the ratio intensity is lower for [110] than for [100], matching our experimental results. In contrast, for FM coupling I_b/I_t is smaller for the [100] direction than for [110]. This calculation helps us to conclude that our samples present an AF coupling between Fe layers in agreement with SQUID measurements. We have calculated a coupling strength of 30 μJ m^{-2} for $t_{ZnSe} = 31$ Å and 46 μJ m^{-2} for $t_{ZnSe} = 25$ Å (figure 4). For samples with $t_{ZnSe} \geqslant 40$ Å we measured a tiny shift of the intensities ratio which would also suggests the existence of an AF coupling. However, due to the fact that the modes keep their relative position and due to the small roughness of the Fe layers, we are not able to derive with accuracy the coupling strength for these samples and thus these results have not been included in figure 4. The minor loop displacements observed in SQUID measurements confirm that the AF coupling persists for thickness up to 80 Å. In this sense, FMR and SQUID results are complementary, allowing us to deduce the magnetic coupling between iron layers for a wide range of barrier thicknesses.

4. Discussion

Our results provide evidence for the existence of a temperature-dependent antiferromagnetic coupling between iron layers, across a crystalline ZnSe semiconducting barrier. Extrinsic mechanisms such as pinholes and dipolar fields may induce a magnetic coupling across non-magnetic spacers. However, a direct coupling through pinholes has been discarded due to the antiferromagnetic nature of the measured interaction.

In the thin-film geometry, the magnitude of the magnetostatic coupling for ideal and smooth layers is vanishingly small. Nevertheless, the magnetostatic coupling becomes significant if a surface roughness is considered. Steps, ripples and other features of the magnetic layers surface result in stray magnetic field lines that couple neighbouring layers; i.e., the so-called Orange-Peel (OP) or Néel coupling. This coupling leads to an effective ferromagnetic or antiferromagnetic field depending on the roughness topology. We have calculated the OP coupling strength for the Fe/ZnSe/Fe trilayers. TEM and STM images allow us to estimate the roughness amplitude at the different interfaces ZnSe/Fe_b, Fe_b/ZnSe barrier, ZnSe barrier/Fe_t, Fe_t/cover ZnSe of the structure. The calculation was performed for the worst situation, that is

assuming one monolayer roughness at the Fe_b/ZnSe barrier and the Fe_t/ZnSe barrier interfaces, with a wavelength of 500 Å. This amplitude is increased to 10 Å for the outer Fe interface of the top layer. The ZnSe/Fe_b interface is very flat, so no roughness at this interface has been considered in the calculation of the coupling. Using the formula given in [34] and the roughness parameters mentioned above, the OP coupling strength results to be 14 μJ m^{-2}. The coupling is of the same order of magnitude as the measured one, but is ferromagnetic and therefore does not match our results. Moreover, this effective dipolar coupling is proportional to the magnetization of the magnetic layer, which decreases with increasing temperature. Thus, the OP coupling is expected to decrease with increasing temperature, and so it cannot explain the temperature dependence of coupling measured in our samples. A variation of less than 2% in the OP coupling is expected for the temperature range of our measurements.

Hence, we have explored theoretical models based on intrinsic coupling mechanisms to analyse our results. Bruno proposed, in [2], an extension of his former RKKY interlayer coupling model for metallic and insulating barriers. In spite of the unified treatment, the thickness and temperature dependences of the coupling are drastically different in both cases. The coupling dependence with spacer thickness is oscillatory in metallic structures while it decreases exponentially in the case of an insulator barrier. Bruno deduced the existence of an antiferromagnetic coupling for spacer thickness $t > 10$ Å. The coupling strength decays rapidly from 10 μJ m^{-2} to zero, as the barrier thickness is increased from 12 to 23 Å. It is important to note that Bruno's calculations were performed for relatively low barriers ($U - \varepsilon_F = 0.1$ eV) and assuming that the electrons that mediate the coupling have a s-character. Similar calculations using adequate parameters for the Fe/MgO/Fe system ($U - \varepsilon_F = 1$ eV) were performed by Faure-Vincent *et al* [18]. These authors find that the system is antiferromagnetically coupled for spacers thinner than ∼8 Å, with a maximum strength of 300 μJ m^{-2} at 5 Å. The barrier height of our samples is higher than the value used for Bruno's calculations, but quite close to the value used in [18]. According to our previous photoemission experiments [35], the Fe Fermi level position is stabilized at 1.6 eV above the valence-band maximum of undoped ZnSe, i.e., a barrier height of $U - \varepsilon_F = 1.1$ eV. Our results agree qualitatively with the spacer thickness dependence of the coupling strength predicted by Bruno's model; i.e., we have found a strong decrease of the antiferromagnetic coupling strength with the ZnSe spacer thickness. Nevertheless, the variation of the coupling strength with the spacer thickness dependence is much smoother than the predicted behaviour.

The temperature dependence of the antiferromagnetic coupling, depicted in figure 5, does not seem to show the rapid increase with temperature reported in [2]. The exchange coupling measured for our samples increases linearly with increasing temperature. However, we want to remark that the increase of coupling strength with temperature reported by Bruno is notably sharp only above room temperature. In this sense, the variation of the IEC with temperature measured for our samples does not differ qualitatively from the model reported in [2].

Walser and co-workers report in [13] measurements of a thermally induced antiferromagnetic exchange coupling across an amorphous ZnSe barrier of thickness varying from 18 to 25 Å. The coupling changes to ferromagnetic below 15 Å and above 30 Å at any investigated temperature. The magnitude of the antiferromagnetic exchange coupling strength is very small (<18 μJ m^{-2}), exhibiting a thermal saturation above ∼100 K. In our samples that have crystalline ZnSe spacers, the magnitude of the antiferromagnetic coupling strength is much larger at room temperature and presents no evidence of thermal saturation. We have studied samples with thicker ZnSe spacer thicknesses to minimize the effect of extrinsic factors such as layer thickness fluctuations due to interface waviness, crystal/interface quality and pinholes. The thickness waviness and pinhole formation seem to be more critical in our epitaxial structures than in samples with amorphous spacers. Hunziker *et al*

analyse the coupling measured in their samples in terms of large molecular orbitals, built along the spacer layer [25]. This explanation is not suitable for our case because in our samples the defect/impurity density is lower and the spacer thickness range is much larger compared to those found for a-ZnSe. Although in a recent work we have demonstrated that resonant tunnelling via localized states through ZnSe barriers is effectively important to explain the magnetoresistance in Fe/ZnSe/Fe planar junctions fabricated from Fe/ZnSe/Fe heterostructures prepared under the same growth conditions [36], it seems that the thermally induced antiferromagnetic exchange coupling proposed by Landolt's group cannot be simply extended to explain our present results.

We have also analysed the double-quantum-well model proposed by Hu and co-workers [37] to explain the exchange coupling in trilayered Fe/ZnSe/Fe structures. These authors report the existence of two kind of interlayer couplings, a resonant and a non-resonant one. The first is, alternatively, ferromagnetic and antiferromagnetic, changing sign without a definite periodicity but depending on the ferromagnetic layer thickness. The coupling strength varies from -1000 μJ m^{-2} to 2500 m^2 as the iron layer thickness varies from 0 to 200 Å, keeping the barrier thickness constant at 10 Å. The non-resonant J is much smaller than the resonant one (less than 1 μJ m^{-2}) and varies drastically with the iron thickness. The calculated coupling strength for both cases is different from the measured in our samples. Moreover, the resonant case is observed for very thin magnetic layers which is not so in our case.

5. Conclusions

We have presented experimental evidence of magnetic coupling through a semiconducting barrier in the Fe/ZnSe/Fe system. The samples were epitaxially grown by MBE and display very small surface roughness. A weak antiferromagnetic coupling between the iron layers across the crystalline ZnSe barrier was measured through magnetization loop shifts and FMR experiments. The coupling strength measured in the samples with thinner spacer is of the order of $\sim$10 μJ m^{-2}, being, at least, 10 times weaker than coupling in metallic spacer system [38].

The Orange-Péel dipolar coupling calculated for the samples is always ferromagnetic and is thus ruled out as the origin of our results. We have explained our results in terms of an intrinsic magnetic coupling through the non-metallic barrier by spin-polarized quantum tunnelling of electrons. The thickness and temperature dependences of the magnetic coupling agree with theoretical models proposed for these structures [2].

As a particular challenge, we propose the tailoring of the epitaxial growth of this system and other ferromagnetic/semiconductor/ferromagnetic systems in order to investigate the exchange coupling in a wide spacer thickness range and variable magnetic layer thickness by applying a bias voltage to control thermal excitations and population of the electronic states in the spacer.

Acknowledgments

The authors are grateful for partial financial support from bilateral program Capes-Cofecub, ACI-Nanosciences, CNPq, FAPESP (grants 03/09933-8 and 04/08524-0), ANPCYT (PICT No 3-6340), CONICET (PIP No 2626) and Fundación Antorchas. JM acknowledges support given by the PICS: 'Structure, Morphologie et Magnétisme des systèmes de dimension réduite' between France and Argentina. JM thanks A Butera for fruitful discussion and also thanks J Pérez and R Benavídez for technical assistance. LBS and JM are members of CONICET, Argentina.

References

[1] Parkin S S P, Bhadra R and Roche K P 1991 *Phys. Rev. Lett.* **66** 2152
[2] Bruno P 1994 *Phys. Rev.* B **49** 13231
Bruno P 1995 *Phys. Rev.* B **52** 411
[3] Mathon J, Villeret M, Umerski A, Muniz R B, d'Albuquerque e Castro L and Edwards D M 1997 *Phys. Rev.* B **56** 11797
[4] Himpsel F J, Ortega J E, Mankey G J and Willis R F 1998 *Adv. Phys.* **47** 511
[5] Bloemen P J H, Johnson M T, van de Vorst M T H, Coehoorn R, de Vries J J, Jungblut R, aan de Stegge J, Reinders A and de Jonge W J M 1994 *Phys. Rev. Lett.* **72** 764
[6] Okuno S N and Inomata K 1994 *Phys. Rev. Lett.* **72** 1553
[7] Kawakami R K, Rotenberg E, Escorcia-Aparicio E J, Choi H J, Wolfe J H, Smith N V and Qiu Z Q 1999 *Phys. Rev. Lett.* **82** 4098
[8] Carbone C, Vescovo E, Arder O, Gudat W and Everhardt W 1993 *Phys. Rev. Lett.* **71** 2805
[9] Yu D H and Donath M 2003 *Europhys. Lett.* **63** 729
[10] Persat N and Dinia A 1997 *Phys. Rev.* B **56** 2676
[11] Briner B and Landolt M 1994 *Phys. Rev. Lett.* **73** 340
[12] Walser P, Schleberger M, Fuchs P and Landolt M 1998 *Phys. Rev. Lett.* **80** 2217
[13] Walser P, Hunziker H, Spek T and Landolt M 1999 *Phys. Rev.* B **60** 4082
[14] Smits C J P, Filip A T, Swagten H J M, Koopmans B, de Jonge W J M, Chernyshova M, Kowalczyk L, Grasza K, Szczerbakow A, Story T, Palosz W and Sipatov A Yu 2004 *Phys. Rev.* B **69** 224410
[15] Matsukura F, Akiba N, Shen A, Ohno Y, Oiwa A, Katsumoto S, Yye Y and Ohno H 1998 *Physica* B **258** 573
[16] Chiba D, Akiba N, Matsukura F, Ohno Y and Ohno H 2000 *Appl. Phys. Lett.* **77** 1873
[17] Gareev R R, Pohlmann L L, Stein S, Burgler D E, Grungerg P A and Siegel M 2003 *J. Appl. Phys.* **93** 8038
[18] Faure-Vincent F, Tiusan C, Bellouard C, Popova E, Hehn M, Montaigne F and Schuhl A 2002 *Phys. Rev. Lett.* **89** 107206
Faure-Vincent J, Tiusan C, Bellouard C, Popova E, Hehn M, Montaigne F and Schuhl A 2003 *J. Appl. Phys.* **93** 7519
[19] Marangolo M, Gustavsson F, Eddrief M, Sainctavit Ph, Etgens V H, Cros V, Petroff F, George J-M, Bencok P and Brookes N B 2002 *Phys. Rev. Lett.* **88** 217202
[20] Carbonell L, Etgens V H, Koëbel A, Eddrief M and Capelle B 1999 *J. Cryst. Growth* **201/202** 502
[21] Etgens V H, Capelle B, Carbonell L and Eddrief M 1999 *Appl. Phys. Lett.* **75** 2108
[22] Varalda J, Ribeiro G A P, Ortiz W A, de Oliveira A J A, Mosca D H, Etgens V H and Eddrief M 2002 *Physica* B **322** 312
[23] Steren L B, Milano J, Eddrief M and Etgens V H 2002 *Physica* B **320** 162
[24] Bertacco R, Riva M, Cantoni M, Ciccacci F, Portalupi M, Brambilla A, Duò L, Vavassori P, Gustavsson F, George J-M, Marangolo M, Eddrief M and Etgens V H 2004 *Phys. Rev.* B **69** 054421
[25] Marangolo M, Gustavsson F, Guichar G M, Eddrief M, Varalda J, Etgens V H, Rivoire M, Gendron F, Magnan H, Mosca D H and George J-M 2004 *Phys. Rev.* B **70** 134404
[26] Hunziker M and Landolt M 2000 *Phys. Rev. Lett.* **84** 4713
[27] Drechal V, Kudrnovsky J, Bruno P, Turek I, Dederichs P H and Weinberger P 1999 *Phys. Rev.* B **60** 9588
[28] Layadi A and Artman J O 1990 *J. Magn. Magn. Mater.* **92** 143
[29] Brockmann M, Zölfl M, Miethaner S and Bayreuther G 1999 *J. Magn. Magn. Mater.* **198/199** 384
Reiger E, Reinwald E, Garreau G, Ernst M, Zölfl M, Bensch F, Bauer S, Preis H and Bayreuther G 2000 *J. Appl. Phys.* **87** 5923
da Silva E C, Meckenstock R, von Geisau O, Kordecki R, Pelzl J, Wolf J O and Grünberg P 1993 *J. Magn. Magn. Mater.* **121** 528
[30] Smit J and Beljers H G 1955 *Philips Res. Rep.* **10** 113
[31] Ament W S and Rado G T 1955 *Phys. Rev.* **97** 1558
[32] Cochran J F, Heinrich B and Arrott A S 1986 *Phys. Rev.* B **34** 7788
[33] Kittel C and Herring C 1950 *Phys. Rev.* **77** 725
[34] Kools C S, Kula W, Mauri D and Lin T 1999 *J. Appl. Phys.* **85** 4466
[35] Eddrief M, Marangolo M, Corlevi S, Guichar G M, Etgens V H, Mattana R, Mosca D H and Sirotti F 2002 *Appl. Phys. Lett.* **81** 4553
[36] Varalda J, de Oliveira A J A, Mosca D H, George J-M, Eddrief M, Marangolo M and Etgens V H 2005 *Phys. Rev.* B **72** 081302(R)
[37] Hu N, Wang J Z and Li B Z 2001 *J. Phys.: Condens. Matter* **13** L215
[38] Zhang Z, Zhou L, Wigen P E and Ounadjela K 1994 *Phys. Rev.* B **50** 6094